crystals

MDPI

Article

Anomalous Dynamics of Recalescence Front in Crystal Growth Processes: Theoretical Background

Dmitri V. Alexandrov [1], Peter K. Galenko [1,2,*] and Liubov V. Toropova [2,3]

[1] Laboratory of Multi-Scale Mathematical Modeling, Department of Theoretical and Mathematical Physics, Ural Federal University, Lenin Ave., 51, Ekaterinburg 620000, Russia
[2] Otto-Schott-Institut für Materialforschung, Friedrich-Schiller-Universität-Jena, 07743 Jena, Germany
[3] Laboratory of Mathematical Modeling of Physical and Chemical Processes in Multiphase Media, Department of Theoretical and Mathematical Physics, Ural Federal University, Lenin Ave., 51, Ekaterinburg 620000, Russia
* Correspondence: peter.galenko@uni-jena.de

Abstract: A theory for crystal nucleation and growth with the recalescence front is developed. The theory is based on the saddle-point technique for evaluating a Laplace-type integral as well as the small parameter method for solving the moving boundary heat transfer problem. The theory developed shows the U-shaped behavior of the growth velocity–melt undercooling curve. The ordinary upward branch of this curve is caused by the growth dictated by heat transport and the predominant crystal growth, while the unusual downward branch demonstrates the anomalous behavior caused by the predominant nucleation and attachment kinetics of the growing crystals to the phase interface. Such a U-shaped behavior of the growth velocity–melt undercooling curve is consistent with experimental data carried out on the ground, under reduced gravity during parabolic flights, and in the microgravity conditions onboard the International Space Station [M. Reinartz et al., JOM 74, 2420 (2022); P.K. Galenko et al., Acta Mater. 241, 118384 (2022)].

Keywords: recalescence front; anomalous dynamics; moving boundary problem; solidification; nucleation; crystal growth; undercooling

Citation: Alexandrov, D.V.; Galenko, P.K.; Toropova, L.V. Anomalous Dynamics of Recalescence Front in Crystal Growth Processes: Theoretical Background. *Crystals* **2022**, *12*, 1686. https://doi.org/10.3390/cryst12121686

Academic Editors: Petros Koutsoukos, Andrew Kao and Catherine Tonry

Received: 30 October 2022
Accepted: 20 November 2022
Published: 22 November 2022

1. Introduction

The solid–liquid interface dynamics in the phase transformation processes from an undercooled liquid to a solid state completely determine the direction and velocity of crystallization as well as the properties of the solidifying material. A mathematical model of such a process was first formulated in Stefan's pioneering works [1,2], and the thermodiffusion problem with a moving phase transformation interface is now called the Stefan problem [3–5]. In general, a non-stationary Stefan-type problem with a moving curved boundary of the phase transformation (crystallization front) has no exact analytical solution. As this takes place, one can find a single integro-differential equation for the interface function that defines the time-dependent position of a curvilinear crystallization front. This approach, or the boundary integral theory, is based on Green's function technique [6–9]. However, a direct solution of a thermodiffusion differential model with a moving phase transformation interface or the boundary integral equation can be solved analytically only in cases of quasi-stationary interface growth having a known shape (i.e., planar, spherical, or paraboloidal) [10–15]. In natural processes and technological conditions, the crystallization phenomenon can be complicated by the fact that the liquid phase (solution or melt) before the solid/liquid phase interface may contain microcrystals from the solid phase. In this case, a simultaneous effect of growth and the nucleation of crystals exists during crystallization [16–21]. This effect leads, for example, to the U-shape behavior of the recalescence front velocity–melt undercooling curve [20,21]. At a glance, such behavior seems to be non-trivial. To explain why the front velocity decreases and increases with undercooling,

we need to describe the process of crystal nucleation within a thin, undercooled two-phase layer ahead of the phase interface. This theory is developed below.

This paper is organized as follows: A theoretical model describing the nucleation and growth of crystals in an undercooled two-phase layer is given in Section 2 based on classical nucleation theory [22–28]. A numerical example of the nucleation and growth of crystals is considered in Section 3, where the interface motion is analyzed for the obtained driving force (melt undercooling). Our conclusions are formulated in Section 4.

2. Theoretical Modeling

In this section, we formulate the integro-differential model describing the evolution of a crystal assemblage in an undercooled liquid and obtain an analytical solution to this model using the small parameter method.

2.1. The Model of Crystal Ensemble Nucleation

We consider a single-component melt that occupies a half-space $\xi > 0$. At the time $\tau = 0$, the melt's initial temperature T_l is higher than the temperature of the phase transition T_p. Then, the boundary temperature at $\xi = 0$ goes to a value of $T_0 < T_p$. As a result of heat transfer, the undercooling temperature $\Delta T = T_p - T$ goes into the liquid phase, occupying the region $0 < \xi < \Sigma(\tau)$. Here, τ is the time variable, and $\Sigma(\tau)$ is the moving phase transition boundary, where $T = T_l = T_p$ (T and T_l denote temperatures in the regions $0 < \xi < \Sigma(\tau)$ and $\xi > \Sigma(\tau)$, respectively). Solid-phase nuclei occur at a rate of $I(\Delta T)$ in the undercooled layer $0 < \xi < \Sigma(\tau)$. Note that the undercooling $\Delta T = 0$ at the phase transition boundary $\xi = \Sigma(\tau)$. In addition, the latent heat released during the phase transition reduces the undercooling but does not entirely compensate for it (see Figure 1).

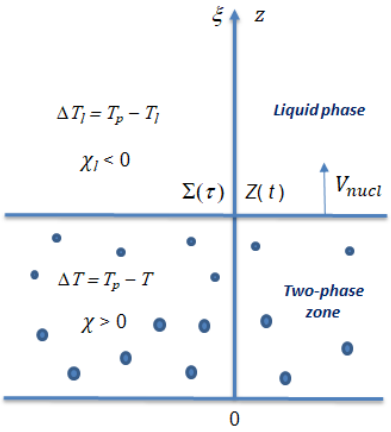

Figure 1. An illustration of the phase transition process where nucleation and growth of crystallites of different sizes (filled circles) are taking place. The crystallization process moving with velocity V_{nucl} is directed along the spatial axis ξ. The two-phase layer–liquid phase boundary $\Sigma(\tau)$ moves due to the predominant nucleation of crystals. Symbols z and $Z(t)$ designate dimensionless values of ξ and $\Sigma(\tau)$, respectively. The dimensionless melt undercooling in the two-phase layer ($\chi = \Delta T/\Delta T_0$) and liquid phase ($\chi_l = \Delta T_l/\Delta T_0$) becomes zero at the phase transition boundary $\xi = \Sigma(\tau)$ (or $z = Z(t)$). Here, T_p and T_0 are the phase transition and initial temperatures, respectively; T and T_l are the current temperatures in the two-phase layer and liquid phase, respectively.

Further, we assume the quasi-stationary growth velocity of single spherical crystals [29–32], i.e.,

$$\frac{dr}{d\tau} = \frac{\beta_* \Delta T}{1 + \beta_* q r}, \tag{1}$$

where r is the crystal radius, β_* is the kinetic parameter, and $q = \frac{L_V}{\lambda_l}$ with L_V representing the latent heat of the crystallization and λ_l as the thermal conductivity of the liquid. Let

us note that Expression (1) can be derived when considering the stationary temperature conductivity equation in liquid. Note as well that a generalization of the growth law (1) to the unsteady temperature field around the growing crystal can be constructed. Such a generalization has been completed in Refs. [33–35] for undercooled single/binary melts and supersaturated solutions.

There are two modes of crystal growth that depend on the particle radius r. When it is small enough, $r \ll \frac{1}{\beta_* q}$, the crystal growth rate does not depend on r, and the growth mode can be called "kinetic"; however, when the rate of particle growth is controlled by the rate of heat removal, $r \gg \frac{1}{\beta_* q}$, the regime is called "diffusion-controlled growth".

Let us consider the well-known nucleation rate that depends only on melt undercooling [36]

$$I(\Delta T) = \begin{cases} I_* \exp\left[-p\left(\frac{\Delta T_0}{\Delta T}\right)^2\right], \text{ WVFZ kinetics} \\ I_*(\Delta T)^p, \text{ Meirs kinetics} \end{cases}, \quad (2)$$

where the acronym WWFZ means the Weber–Volmer–Frenkel–Zeldovich nucleation kinetics, I_* is the pre-exponential factor, and ΔT_0 represents the initial undercooling of the melt [36]. Parameter $p = \frac{16\pi\gamma_i^3 T_p}{3L_V^2 \Delta T_0^2 k_B}$ (where γ_i is the surface tension, and k_B is the Boltzmann constant) is a dimensionless Gibbs number in the case of the WVFZ kinetics and an empirical constant in the case of the Meirs kinetics.

The particle-radius distribution function $\phi(\tau, \xi, r)$ in the moving two-phase layer filled with nucleating and growing crystals satisfies the kinetic equation

$$\frac{\partial \phi}{\partial \tau} + \frac{\partial}{\partial r}\left(\frac{dr}{d\tau}\phi\right) = 0,\ 0 < \xi < \Sigma(\tau),\ r > 0,\ \tau > 0. \quad (3)$$

The temperature field in the moving layers $0 < \xi < \Sigma(\tau)$ and $\xi > \Sigma(\tau)$ is defined by the heat transfer equations

$$\rho c \frac{\partial T}{\partial \tau} = \lambda \frac{\partial^2 T}{\partial \xi^2} + \frac{4\pi L_V}{3} \frac{\partial}{\partial \tau} \int_0^\infty r^3 \phi dr,\ 0 < \xi < \Sigma(\tau),\ \tau > 0, \quad (4)$$

$$\rho_l c_l \frac{\partial T_l}{\partial \tau} = \lambda_l \frac{\partial^2 T_l}{\partial \xi^2},\ \xi > \Sigma(\tau),\ \tau > 0. \quad (5)$$

Here, ρ and ρ_l represent the densities of the two-phase layer and liquid phase, c and c_l define their heat capacities, and λ and λ_l determine their heat conductivity coefficients, respectively, where subscript l designates the liquid layer. Note that newly born crystals within the layer $0 < \xi < \Sigma(\tau)$ release latent crystallization heat, leading to the integral source term in Equation (4).

These equations need to be completed by the boundary and initial conditions at $r = 0$, $\tau = 0$, $\xi = 0$, and $\xi \to \infty$, as well as the phase transition boundary $\xi = \Sigma(\tau)$ of the form

$$\frac{dr}{d\tau}\phi = I(\Delta T),\ r = 0,\ \tau > 0;\ \phi = 0,\ \tau = 0,\ 0 < \xi < \Sigma(\tau); \quad (6)$$

$$T = T_0,\ \xi = 0,\ \tau > 0;\ T_l \to T_\infty,\ \xi \to \infty, \tau > 0; \quad (7)$$

$$T = T_l = T_p,\ \frac{\partial T}{\partial \xi} = \frac{\partial T_l}{\partial \xi},\ \xi = \Sigma(\tau),\ \tau > 0;\ T_l = T_\infty,\ \tau = 0. \quad (8)$$

2.2. Analytical Solution

For convenience, we use the following dimensionless values

$$\begin{gathered} D_f = \ell^4\phi,\ \sigma = \tfrac{r}{\ell},\ z = \tfrac{\xi}{\ell}, \chi = \frac{\Delta T}{\Delta T_0},\ \chi_l = \frac{\Delta T_l}{\Delta T_0}, \\ \gamma = \tfrac{\lambda\tau_o}{\rho c\ell^2},\ Z = \frac{\Sigma}{\ell},\ t = \frac{\tau}{\tau_o},\ b = \frac{4\pi L_V}{3\rho c\Delta T_0}, \\ \alpha_* = \beta_* q\ell, \tau_o = \frac{\ell}{\beta_k \Delta T_0}, \ell = \left(\frac{\beta_k \Delta T_0}{I_0}\right)^{1/4}, \end{gathered} \tag{9}$$

where $\Delta T_0 = T_p - T_0$ and $\Delta T_l = T_p - T_l$ are the initial and current undercoolings, respectively. Let us specifically highlight that D_f represents the dimensionless particle-radius distribution function, σ stands for the dimensionless radius of the crystals, z represents the dimensionless crystallization axis plotted in Figure 1, t is the dimensionless time variable, and χ and χ_l mean the dimensionless undercoolings in the layer of nucleation $0 < z < Z(t)$ and the liquid phase $z > Z(t)$.

Rewriting now the model expressions and boundary conditions in dimensionless variables, we arrive at the kinetic equation and the boundary and initial conditions for the dimensionless distribution function D_f in a two-phase layer $0 < z < Z(t)$, which reads as

$$\frac{\partial D_f}{\partial t} + \chi \frac{\partial}{\partial \sigma}\left(\frac{D_f}{1+\alpha_*\sigma}\right) = 0,\ \sigma > 0,\ t > 0, \tag{10}$$

$$D_f = \frac{1}{\chi}\exp[pg(\chi)],\ \sigma = 0;\ D_f = 0,\ t = 0, \tag{11}$$

where

$$g(\chi) = g(t,z) = \begin{cases} 1 - \chi^{-2}, \text{ WVFZ nucleation kinetics} \\ \ln\chi, \text{ Meirs nucleation kinetics} \end{cases}. \tag{12}$$

Applying the Laplace integral transform to the model (10) and (11) regarding t, we obtain the distribution function of particles along the radius in the form of

$$D_f = (1+\alpha_*\sigma)\varphi(x(t,z) - y(\sigma))\eta(x(t,z) - y(\sigma)), \tag{13}$$

where

$$\varphi(t,z) = \frac{1}{\chi}\exp(pg(t,z)),\ x(t,z) = \int_0^t \chi(t_1,z)dt_1,\ y(\sigma) = \sigma + \frac{\alpha_*\sigma^2}{2}, \tag{14}$$

and η represents the Heaviside function.

Then, substituting the dimensionless parameters and variables (9) into Expressions (4) and (5) and the boundary conditions (7) and (8), we obtain

$$\frac{\partial \chi}{\partial t} = \gamma\frac{\partial^2\chi}{\partial z^2} - b\frac{\partial}{\partial t}\int_0^t h(\nu,t,z)\exp(pg(\nu,z))d\nu,\ 0 < z < Z(t),\ t > 0, \tag{15}$$

$$\frac{\partial \chi_l}{\partial t} = \gamma\frac{\partial^2\chi_l}{\partial z^2},\ z > Z(t),\ t > 0, \tag{16}$$

$$\chi = 1,\ z = 0,\ t > 0;\ \chi_l \to \chi_\infty = \frac{T_p - T_\infty}{\Delta T_0},\ z \to \infty,\ t > 0; \tag{17}$$

$$\chi = \chi_l = 0,\ \frac{\partial \chi}{\partial z} = \frac{\partial \chi_l}{\partial z},\ z = Z(t),\ t > 0;\ \chi_l = \chi_\infty,\ t = 0, \tag{18}$$

where we suppose that $\rho = \rho_l$, $\lambda = \lambda_l$, and $c = c_l$. We notice that the integral included in the right-hand side of Formula (15) is written according to the previously described theory [36], in which the variable ν fulfills formulas $x(\nu, z) = x(t, z) - y(\sigma)$ and $h(\nu, t, z) = \alpha_*^{-3}\left[\sqrt{1 + 2\alpha_*(x(t,z) - x(\nu,z))} - 1\right]^3$.

The integral term in Expression (15) can be estimated given the fact that the dimensionless variable p is significantly greater than unity for a large variety of undercooled melts [36]. This integral can then be calculated using the saddle-point method for the Laplace integral [37,38]. Equation (12) shows that $\partial g/\partial \nu = (dg/d\chi)\partial\chi/\partial\nu < 0$ for the two kinetic mechanisms under question: the WVFZ and Meirs ($dg/d\chi > 0$ and $d\chi/d\nu < 0$). This is due to the fact that the function g reaches a maximum value at the boundary point $\nu = 0$. Estimating the derivatives χ on ν using Equation (15), we find that the first three of them become zero at $\nu = 0$, and the fourth derivative is $-12b$ in the case of the WVFZ and $-6b$ in the case of the Meirs kinetics. Keeping just the main term of the asymptotic expansion in (15), we obtain [37,38]

$$\frac{\partial \chi}{\partial t} = \gamma \frac{\partial^2 \chi}{\partial z^2} - A\varrho(\chi, t, z),\ t > 0,\ 0 < z < Z(t), \tag{19}$$

where

$$\varrho(t,z) = \frac{\chi(t,z)\left[\sqrt{1 + 2\alpha_* x(t,z)} - 1\right]^2}{\sqrt{1 + 2\alpha_* x(t,z)}},\ A = \frac{3b^{3/4}\Gamma(1/4)}{b_0 \alpha_*^2 p^{1/4}}, \tag{20}$$

and Γ represents the Euler gamma function, $b_0 = 2^{7/4}$ (the WVFZ), and $b_0 = 4^{3/4}$ (the Meirs kinetics).

Let us further discuss two crystal growth modes: the kinetic ($\alpha_* \ll 1$, KG) and diffusion-controlled ($\alpha_* \gg 1$, DCG) ones. For these cases, we obtain from (20)

$$\varrho(t,z) \approx \begin{cases} \alpha_*^2 x^2(t,z)\chi(t,z), \text{ KG} \\ \sqrt{2\alpha_* x(t,z)}\chi(t,z), \text{ DCG.} \end{cases} \tag{21}$$

Now combining expressions (19)–(21), we have

$$\frac{\partial \chi}{\partial t} = \gamma \frac{\partial^2 \chi}{\partial z^2} - \varepsilon\Phi(\chi, x),\ t > 0,\ 0 < z < Z(t), \tag{22}$$

where

$$\varepsilon = \begin{cases} \alpha_*^2 A, \text{ KG} \\ \sqrt{2\alpha_*} A, \text{ DCG} \end{cases} \text{ and } \Phi(\chi, x) = \begin{cases} x^2\chi, \text{ KG} \\ \sqrt{x}\chi, \text{ DCG} \end{cases}. \tag{23}$$

Below, we search for the solution to (16)–(18), (22), and (23) as a power expansion with a small parameter ε

$$\chi = \chi_0 + \varepsilon\chi_1 + ...,\ Z = Z_0 + \varepsilon Z_1 + ... \tag{24}$$

By substituting Formula (24) into Expressions (16) and (22), expanding the boundary conditions at $z = Z(t)$ in the Taylor series, and equating terms with the same power of ε,

we come to the conclusion that the problem can be solved using the following self-similar variables

$$\chi_0 = f_0(\zeta),\ \zeta = \frac{z}{\sqrt{t}},\ Z_0(t) = \alpha\sqrt{t}, \tag{25}$$

$$\chi_1 = \begin{cases} f_1(\zeta)t^3, \text{ KG} \\ f_1(\zeta)t^{3/2}, \text{ DCG} \end{cases} \text{ and } Z_1(t) = \begin{cases} \beta t^{7/2}, \text{ KG} \\ \beta t^2, \text{ DCG} \end{cases}.$$

In this case, α and β are the constant coefficients determining the phase transition boundary $Z(t)$. Functions $f_0(\zeta)$ and $f_1(\zeta)$ will be introduced later. Consequently, the governing equations and boundary conditions, (16)–(18), (22), and (23), can be written as

$$\gamma\frac{d^2f_0}{d\zeta^2} = -\frac{\zeta}{2}\frac{df_0}{d\zeta},\ \gamma\frac{d^2f_1}{d\zeta^2} = \Psi(\zeta) - \frac{\zeta}{2}\frac{df_1}{d\zeta},\ \gamma\frac{d^2\chi_l}{d\zeta^2} = -\frac{\zeta}{2}\frac{d\chi_l}{d\zeta}, \tag{26}$$

$$f_0 = 1,\ f_1 = 0,\ \zeta = 0;\ \chi_l \to \chi_\infty,\ \zeta \to \infty; \tag{27}$$

$$f_0 = 0,\ f_1 + \beta\frac{df_0}{d\zeta} = 0,\ \chi_l = 0,\ \frac{df_0}{d\zeta} = \frac{d\chi_l}{d\zeta},\ \frac{df_1}{d\zeta} = 0,\ \zeta = \alpha, \tag{28}$$

where

$$\Psi(\zeta) = \begin{cases} 4K^2(\zeta)\zeta^4 f_0(\zeta), \text{ KG} \\ \sqrt{2K(\zeta)}\zeta f_0(\zeta), \text{ DCG} \end{cases} \text{ and } K(\zeta) = \int_\zeta^\infty \frac{f_0(\zeta_1)}{\zeta_1^3}d\zeta_1.$$

The analytical solution to the problem presented in (26)–(28) can be expressed as

$$f_0(\zeta) = 1 - \frac{\operatorname{erf}\left(\frac{\zeta}{2\sqrt{\gamma}}\right)}{\operatorname{erf}\left(\frac{\alpha}{2\sqrt{\gamma}}\right)},\ f_1(\zeta) = \int_0^\zeta (\Omega(\zeta_1) - \Omega(\alpha))\exp\left(-\frac{\zeta_1^2}{4\gamma}\right)d\zeta_1, \tag{29}$$

$$\chi_l(\zeta) = \chi_\infty\left[1 - \frac{\operatorname{erfc}\left(\frac{\zeta}{2\sqrt{\gamma}}\right)}{\operatorname{erfc}\left(\frac{\alpha}{2\sqrt{\gamma}}\right)}\right],\ \Omega(\zeta) = \frac{1}{\gamma}\int_0^\zeta \Psi(\zeta_1)\exp\left(\frac{\zeta_1^2}{4\gamma}\right)d\zeta_1. \tag{30}$$

Constants α and β must be found from the following expressions

$$\operatorname{erfc}\left(\frac{\alpha}{2\sqrt{\gamma}}\right) + \chi_\infty\operatorname{erf}\left(\frac{\alpha}{2\sqrt{\gamma}}\right) = 0, \tag{31}$$

$$\beta = \sqrt{\pi\gamma}\operatorname{erf}\left(\frac{\alpha}{2\sqrt{\gamma}}\right)\exp\left(\frac{\alpha^2}{4\gamma}\right)f_1(\alpha). \tag{32}$$

3. Numerical Example

In this section, we obtain the melt undercooling that drives the crystallization process and takes the phase interface motion into account; i.e., we consider a simultaneous process of bulk nucleation and the growth of crystals. In this case, the melt undercooling as well as the crystallization velocity contain two contributions associated with these two process modes.

Since solidification kinetics are experimentally defined by the phenomena of crystal nucleation and growth, the theoretical explanation should include both of these processes as well. Therefore, the process mode contains the two-phase layer with the bulk nucleation of crystals (see Figure 2a). Since, in solidification experiments of undercooled droplets, the whole system shown in Figure 2a is in motion due to the crystal growth of the solid phase

(motion of the recalescence front), we are switching to a moving frame of reference. In this case, we have the combined bulk nucleation and growth of crystals shown in Figure 2b. In other words, the whole growth rate contains two contributions appearing from the bulk nucleation (V_{nucl}) and crystal growth (V_{front}). The recalescence front velocity is given by $V_{rec} = |V_{nucl}| + V_{front}$.

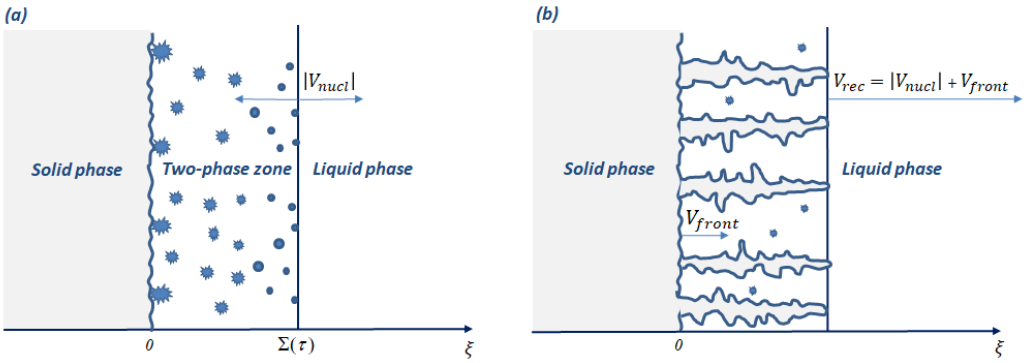

Figure 2. An illustration showing the moving two-phase zone along the spatial coordinate ξ at time τ. Panel (**a**) demonstrates the bulk phase transition process described in Section 2. Panel (**b**) illustrates a combined effect of the bulk and crystallization from an undercooled melt.

For the sake of convenience, we use dimensional variables to describe the main parameters that characterize the motion of the recalescence front: its growth velocity V_{rec}, time τ, and the melt undercooling ΔT. First, we define the undercooling balance ΔT as the sum of nucleation and the front undercoolings

$$\Delta T = \Delta T_{nucl} + \Delta T_{front}, \tag{33}$$

$$\Delta T_{nucl} = \Delta T_0 \left[f_0(\xi, \tau) + \varepsilon I_0^{k/4} \beta_*^{3k/4} \Delta T_0^{3k/4} \tau^k f_1(\xi, \tau) \right], \tag{34}$$

$$\Delta T_{front} = \left(\frac{V}{\mu_k} \right)^{1/l}, \tag{35}$$

where μ_k is the kinetic coefficient for undercooling, and l is a constant parameter. The velocity of the recalescence front reads as

$$V_{rec} = |V_{nucl}| + V_{front}, \tag{36}$$

$$V_{nucl} = \left(\frac{\beta_* \Delta T_0}{I_0} \right)^{1/4} \left[\frac{\alpha I_0^{1/8} \beta_*^{3/8} \Delta T_0^{3/8}}{2\sqrt{\tau}} + \frac{7}{2} \varepsilon \beta \tau^{5/2} I_0^{7/8} \beta_*^{21/8} \Delta T_0^{21/8} \right], \tag{37}$$

$$V_{front} = \mu_k \Delta T^l. \tag{38}$$

Here, Expressions (34) and (37) follow from Equation (24).

In previous studies [20,21,39,40], anomalous behavior of the "melt undercooling–recalescence front velocity" curve was observed using electromagnetic levitation experiments for the Al-rich Al-Ni alloys. Namely, a decreasing branch of the solidification (recalescence front) velocity for the increasing melt undercooling was detected. Below, we explain this behavior using an active nucleation process ahead of the growing solid phase.

Our calculations, based on the model under question in kinetic growth mode, have shown that the nucleation front velocity V_{nucl} gradually decreases with time and changes its sign from positive to negative (Figure 3). In this pure nucleation growth mode, shown in Figure 2a, the process has two stages. During the first of these, Stage (i), the crystals actively nucleate and start to grow ($\Sigma(\tau)$ increases with time and $V_{nucl}(\tau) > 0$). During the second stage, which is Stage (ii), the crystals already release a sufficient amount of the latent crystallization heat and thus partially compensate for the melt undercooling ($\Sigma(\tau)$ decreases with time and $V_{nucl}(\tau) < 0$). When dealing with the simultaneous operation of bulk nucleation and crystal growth (Figure 2b), the solid-phase–two-phase zone boundary is moving with the velocity V_{front} induced by the driving force similar to what occurs during the solidification of undercooled droplets in an electromagnetic levitation facility. From the physical point of view, we are shifting to the reference frame moving at the speed V_{front} in Figure 2a and thus obtaining the combined process illustrated in Figure 2b. In this case, as before, we have the two aforementioned stages of the combined process of bulk nucleation and the growth of crystals. When dealing with Stage (i), the recalescence front velocity V_{rec} is a sum of two additive contributions connected with the front propagation due to bulk nucleation, V_{nucl}, and the crystal growth V_{front}. When dealing with Stage (ii), the velocity V_{nucl} is directed towards the front, which is accelerated by the effect of the crystals sticking to the interfacial boundary. As a result, the recalescence front velocity V_{rec} is also the sum of V_{front} and $|V_{nucl}|$. Therefore, we have (36) in both cases.

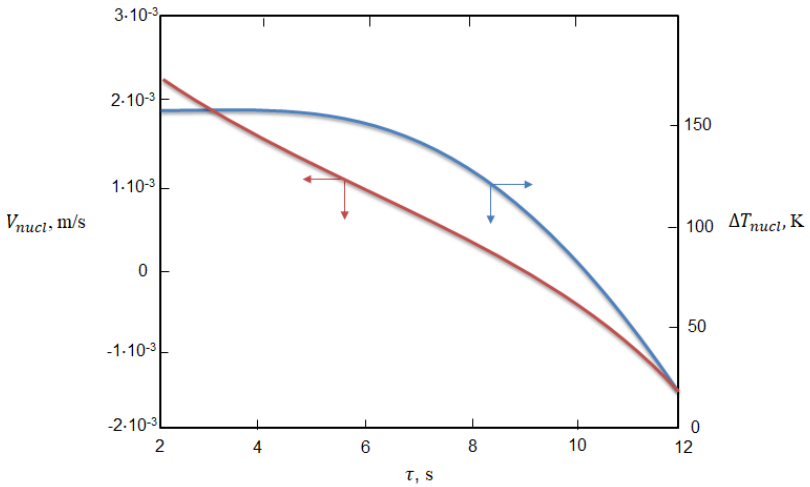

Figure 3. The bulk crystallization velocity V_{nucl} (red line) and melt undercooling ΔT_{nucl} (blue line) as functions of time τ for pure nucleation mode. Physical parameters used for calculations are: $\Delta T_0 = 400$ K, $I_0 = 10^{11}$ m^{-3} s^{-1}, $\beta_* = 2 \cdot 10^{-7}$ m s^{-1} K^{-1}, $\tau_0 = 2.1$ s, $\zeta = 10^{-4}$ m, $\varepsilon = 0.1$, $\alpha = 52.46$, $\beta = 0.1$, $k = 1$, $\gamma = 3 \cdot 10^3$, $p = 8$.

Eliminating the time variable τ from the blue and red curves, $V_{nucl}(\tau)$ and $\Delta T_{nucl}(\tau)$, plotted in Figure 3, we obtain $V_{nucl}(\Delta T)$. By adding $V_{front}(\Delta T)$ from Equation (38) to this relationship, we come to the U-shaped curve $V_{rec}(\Delta T)$ demonstrated in Figure 4. Its minimum point (marked by the vertical dotted line in Figure 4) divides two different regimes of the crystallization process: (i) frontal growth + nucleating crystals ahead of the front and (ii) frontal growth accelerated by the attachment kinetics of particles sticking to the phase interface. The second stage is connected to the narrowing of the nucleation region due to a partial reduction in the melt undercooling as the crystals grow and release latent solidification heat. The theory under consideration qualitatively describes the experimental data for Al-rich Al-Ni alloys solidified in the electromagnetic levitation facility on the ground, under reduced gravity during parabolic flights, and under microgravity conditions onboard the International Space Station [20,21,39,40].

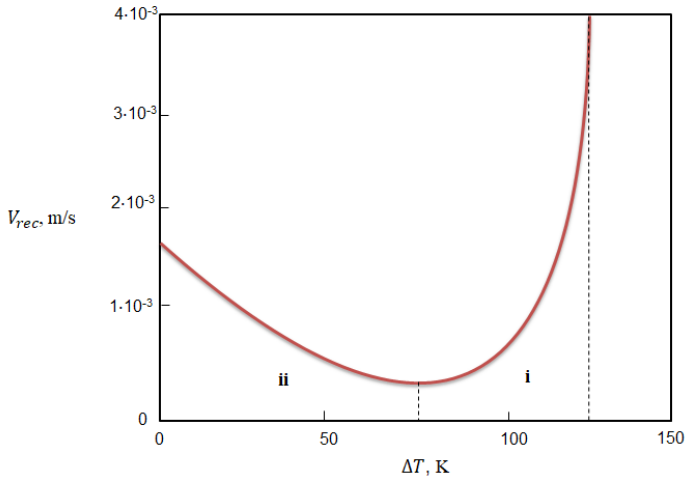

Figure 4. The recalescence front velocity V_{rec} as a function of melt undercooling ΔT. Region (i) describes predominant crystal growth in comparison to the nucleation of crystals ahead of the phase interface while Region (ii) corresponds to propagation of the recalescence front due to predominant contribution of nucleation of crystals over their growth (with the attachment of crystals to the phase interface). Physical parameters used for calculations correspond to Figure 3 and $l = 1$, $\mu_k = 5 \cdot 10^{-6}$ m s^{-1} K^{-1}.

4. Conclusions

In summary, a model of combined bulk nucleation and crystal growth is developed to describe the evolution of the recalescence front. To do this, we first consider a pure bulk crystallization scenario in which newly born crystals grow in the phase transition layer extending/suppressing its thickness Σ with a time τ. This problem, described by the aforementioned integro-differential model, has been solved by the small parameter method. Then, we move the phase transition layer along a spatial direction and thus obtain two contributions: the undercooling balance and the recalescence front velocity $V_{rec} = |V_{nucl}| + V_{front}$ (Figure 2). As a result, the problem of combined bulk nucleation and crystal growth [20] has been described analytically by Expressions (33) and (36). The combined effect of these modes leads to the U-shaped dynamics of the recalescence front velocity. As this takes place, the right (upward) branch in Figure 4 is connected with the predominant crystal growth and intense nucleation mode, and the left (downward) branch describes the predominant nucleation of the crystals with their attachment to the interface. These are due to the fact that the crystals grow and release the latent solidification heat, which partially compensates for the melt undercooling, suppresses the nucleation domain, and induces crystals to stick to the moving front. These two modes of the crystallization process are divided by the minimum point in Figure 4. The U-shaped behavior of the "recalescence front–melt undercooling" curve is in qualitative agreement with the experimental data from Refs. [20,21].

Let us especially note that this paper deals with the anomalous law of motion for the phase transformation boundary resulting from crystallization with a planar front and also nucleation and crystal growth ahead of this front. In many scientific papers devoted to similar problems, the simultaneous operation of these two mechanisms of the crystallization process is not considered (see, among others, [27,41–45]). For a more detailed description of the simultaneous growth and nucleation modes, it is necessary to consider both processes in a non-stationary mode. In other words, to the directional, unsteady crystallization from a cooled wall, one must additionally consider the process of nucleation and bulk crystal growth in front of the crystallization interface (solid phase–two-phase zone interface) [46–50]. To solve such a highly nonlinear problem with a moving boundary, the saddle-point technique can be used to construct an approximate solution to the bulk crystallization problem ahead of the moving interface [26–28], and then the differential series method can be applied to construct an approximate solution to the crystallization problem [33–35]. The

solution to such an urgent problem, which is a subject of future research, is necessary for a more accurate explanation of the U-shaped behavior of the "crystallization velocity–melt undercooling" relationship.

Author Contributions: Conceptualization, D.V.A. and L.V.T.; methodology, D.V.A. and P.K.G.; software, L.V.T. and P.K.G.; validation, L.V.T. and P.K.G.; formal analysis, D.V.A. and P.K.G.; investigation, D.V.A.; resources, P.K.G.; writing—original draft preparation, D.V.A., P.K.G., and L.V.T.; writing—review and editing, D.V.A., L.V.T., and P.K.G.; visualization, L.V.T.; supervision, P.K.G. and D.V.A.; project administration, P.K.G.; funding acquisition, P.K.G. and D.V.A. All authors have read and agreed to the published version of the manuscript.

Funding: This study was supported by the Russian Science Foundation (project no. 21-19-00279).

Data Availability Statement: All data generated or analyzed during this study are included in the published article.

Conflicts of Interest: The authors declare no conflict of interest.

References

1. Stefan, J. Über einige Probleme der Theorie der Wärmeleitung. *Sitzungsberichte Math.–Naturawissenschaftlichen Cl. Der Kais. Akad. Der Wiss.* **1889**, *98*, 473–484.
2. Stefan, J. Über die Theorie der Eisbildung, insbesondere über die Eisbildung im Polarmeere. *Sitzungsberichte Math.–Naturawissenschaftlichen Cl. Der Kais. Akad. Der Wiss.* **1889**, *98*, 965–983. [CrossRef]
3. Meirmanov, A.M. *The Stefan Problem*; De Gruyter Expositions in Mathematics; De Gruyter: Berlin, Germany, 1992.
4. Alexandrov, D.V.; Ivanov, A.A. The Stefan problem of solidification of ternary systems in the presence of moving phase transition regions. *J. Exper. Theor. Phys.* **2009**, *108*, 821–829. [CrossRef]
5. Lee, D.; Alexandrov, D.V. Numerical modeling of one-dimensional binary solidification—The classical two-phase stefan problem. *Int. J. Pure Appl. Math.* **2010**, *58*, 381–416.
6. Nash, G.E.; Glicksman, M.E. Capillary-limited steady-state dendritic growth: I. Theoretical development. *Acta Metall.* **1974**, *22*, 1283–1290. [CrossRef]
7. Langer, J.S.; Turski, L.A. Studies in the theory of interfacial stability: I. Stationary symmetric model. *Acta Metall.* **1977**, *25*, 1113–1119. [CrossRef]
8. Alexandrov, D.V.; Galenko, P.K. Boundary integral approach for propagating interfaces in a binary non-isothermal mixture. *Physica A* **2017**, *469*, 420–428. [CrossRef]
9. Titova, E.A.; Alexandrov, D.V. The boundary integral equation for curved solid/liquid interfaces propagating into a binary liquid with convection. *J. Phys. A Math. Theor.* **2022**, *55*, 055701. [CrossRef]
10. Pelcé, P. *Dynamics of Curved Fronts*; Academic Press: Boston, MA, USA, 1988.
11. Brener, E.A.; Mel'nikov, V.I. Pattern selection in two-dimensional dendritic growth. *Adv. Phys.* **1991**, *40*, 53–97. [CrossRef]
12. Galenko, P.K.; Alexandrov, D.V.; Titova, E.A. The boundary integral theory for slow and rapid curved solid/liquid interfaces propagating into binary systems. *Phil. Trans. R. Soc. A* **2018**, *376*, 20170218. [CrossRef]
13. Toropova, L.V. Shape functions for dendrite tips of SCN and Si. *Eur. Phys. J. Spec. Top.* **2022**, *231*, 1129–1133. [CrossRef]
14. Toropova, L.V.; Alexandrov, D.V.; Rettenmayr, M.; Liu, D. Microstructure and morphology of Si crystals grown in pure Si and Al-Si melts. *J. Phys. Condens. Matter* **2022**, *34*, 094002. [CrossRef]
15. Alexandrov, D.V.; Galenko, P.K. A review on the theory of stable dendritic growth. *Phil. Trans. R. Soc. A* **2021**, *379*, 20200325. [CrossRef]
16. Mansurov, V.V. The nonlinear dynamics of solidification of a binary melt with a nonequilibrium mushy region. *Math. Comput. Model.* **1990**, *14*, 819–821. [CrossRef]
17. Alexandrov, D.V.; Ivanov, A.A.; Alexandrova, I.V. On the theory of bulk crystallization in the moving phase transition layer. *J. Cryst. Growth* **2020**, *532*, 125420. [CrossRef]
18. Alexandrov, D.V.; Dubovoi, G.Y.; Malygin, A.P.; Nizovtseva, I.G.; Toropova, L.V. Solidification of ternary systems with a nonlinear phase diagram. *Russ. Metall. (Met.)* **2017**, *2017*, 127–135. [CrossRef]
19. Makoveeva, E.V.; Alexandrov, D.V. Mathematical simulation of the crystal nucleation and growth at the intermediate stage of a phase transition. *Russ. Metall. (Met.)* **2018**, *2018*, 707–715. [CrossRef]
20. Reinartz, M.; Kolbe, M.; Herlach, D.M.; Rettenmayr, M.; Toropova, L.V.; Alexandrov, D.V.; Galenko, P.K. Study on anomalous rapid solidification of Al-35 at%Ni in microgravity. *JOM* **2022**, *74*, 2420–2427. [CrossRef]
21. Galenko, P.K.; Toropova, L.V.; Alexandrov, D.V.; Phanikumar, G.; Assadi, H.; Reinartz, M.; Paul, P.; Fang, Y.; Lippmann, S. Anomalous kinetics, patterns formation in recalescence, and final microstructure of rapidly solidified Al-rich Al-Ni alloys. *Acta Mater.* **2022**, *241*, 118384. [CrossRef]
22. Skripov, V.P. *Methastable Liquids*; Wiley: New York, NY, USA, 1974.

23. Buyevich, Y.A.; Goldobin, Y.M.; Yasnikov, G.P. Evolution of a particulate system governed by exchange with its environment. *Int. J. Heat Mass Trans.* **1994**, *37*, 3003–3014. [CrossRef]
24. Kelton, K.F.; Greer, A.L. *Nucleation in Condensed Matter: Applications in Materials and Biology*; Elsevier: Amsterdam, The Netherlands, 2010.
25. Alexandrova, I.V.; Alexandrov, D.V. Dynamics of particulate assemblages in metastable liquids: A test of theory with nucleation and growth kinetics. *Phil. Trans. R. Soc. A* **2020**, *378*, 20190245. [CrossRef] [PubMed]
26. Makoveeva, E.V.; Alexandrov, D.V. On the theory of phase transformation process in a binary supercooled melt. *Eur. Phys. J. Spec. Top.* **2020**, *229*, 375–382. [CrossRef]
27. Toropova, L.V.; Makoveeva, E.V.; Osipov, S.I.; Malygin, A.P.; Yang, Y.; Alexandrov, D.V. Nucleation and growth of an ensemble of crystals during the intermediate stage of a phase transition in metastable liquids. *Crystals* **2022**, *12*, 895. [CrossRef]
28. Alexandrov, D.V.; Ivanov, A.A.; Nizovtseva, I.G.; Lippmann, S.; Alexandrova, I.V.; Makoveeva, E.V. Evolution of a polydisperse ensemble of spherical particles in a metastable medium with allowance for heat and mass exchange with the environment. *Crystals* **2022**, *12*, 949. [CrossRef]
29. Strickland-Constable, R.F. *Kinetics and Mechanisms of Crystallization*; Academic Press: London, UK, 1968.
30. Treivus, E.B. *Kinetics of Growth and Dissolution of Crystals*; Leningrad State University: Leningrad, Russia, 1979.
31. Bennema, P. *Industrial Crystallization*; Plenum Press: New York, NY, USA, 1976.
32. Alexandrova, I.V.; Ivanov, A.A.; Malygin, A.P.; Alexandrov, D.V.; Nikishina, M.A. Growth of spherical and ellipsoidal crystals in a metastable liquid. *Eur. Phys. J. Spec. Top.* **2022**, *231*, 1089–1100. [CrossRef]
33. Alexandrov, D.V. Nucleation and evolution of spherical crystals with allowance for their unsteady-state growth rates. *J. Phys. A Math. Theor.* **2018**, *51*, 075102. [CrossRef]
34. Alexandrov, D.V.; Alexandrova, I.V. On the theory of the unsteady-state growth of spherical crystals in metastable liquids. *Phil. Trans. R. Soc. A* **2019**, *377*, 20180209. [CrossRef] [PubMed]
35. Alexandrov, D.V.; Nizovtseva, I.G.; Alexandrova, I.V. On the theory of nucleation and nonstationary evolution of a polydisperse ensemble of crystals. *Int. J. Heat Mass Trans.* **2019**, *128*, 46–53. [CrossRef]
36. Alexandrov, D.V.; Malygin, A.P. Transient nucleation kinetics of crystal growth at the intermediate stage of bulk phase transitions. *J. Phys. A Math. Theor.* **2013**, *46*, 455101. [CrossRef]
37. Fedoruk, M.V. *Saddle-Point Method*; Nauka: Moscow, Russia, 1977.
38. Alexandrov, D.V. Nonlinear dynamics of polydisperse assemblages of particles evolving in metastable media. *Eur. Phys. J. Spec. Top.* **2020**, *229*, 383–404. [CrossRef]
39. Lengsdorf, R.; Holland-Moritz, D.; Herlach, D.M. Anomalous dendrite growth in undercooled melts of Al–Ni alloys in relation to results obtained in reduced gravity. *Scr. Mater.* **2010**, *62*, 365–367. [CrossRef]
40. Herlach, D.M.; Burggraf, S.; Reinartz, M.; Galenko, P.K.; Rettenmayr, M.; Gandin, C.-A.; Henein, H.; Mullis, A.; Ilbagi, A.; Valloton, J. Dendrite growth in undercooled Al-rich Al-Ni melts measured on Earth and in Space. *Phys. Rev. Mater.* **2019**, *3*, 073402-1-7. [CrossRef]
41. Podmaniczky, F.; Gránásy, L. Molecular scale hydrodynamic theory of crystal nucleation and polycrystalline growth. *J. Cryst. Growth* **2022**, *597*, 126854. [CrossRef]
42. McGinty, J.; Yazdanpanah, N.; Price, C.; ter Horst, J.H.; Sefcik, J. Nucleation and crystal growth in continuous crystallization. In *The Handbook of Continuous Crystallization*; The Royal Society of Chemistry: London, UK, 2020; pp. 1–50.
43. Alexandrova, I.V.; Alexandrov, D.V.; Makoveeva, E.V. Ostwald ripening in the presence of simultaneous occurrence of various mass transfer mechanisms: An extension of the Lifshitz–Slyozov theory. *Phil. Trans. R. Soc. A* **2021**, *379*, 20200308. [CrossRef]
44. Makoveeva, E.V.; Alexandrov, D.V. The influence of non-stationarity and interphase curvature on the growth dynamics of spherical crystals in a metastable liquid. *Phil. Trans. R. Soc. A* **2021**, *379*, 20200307. [CrossRef]
45. Gránásy, L.; Tóth, G.I.; Warren, J.A.; Podmaniczky, F.; Tegze, G.; Rátkai, L.; Pusztai, T. Phase-field modeling of crystal nucleation in undercooled liquids—A review. *Prog. Mater. Sci.* **2019**, *106*, 100569. [CrossRef]
46. Alexandrov, D.V. Dynamics of the phase transition boundary in the presence of nucleation and growth of crystals. *J. Phys. A Math. Theor.* **2017**, *50*, 345101. [CrossRef]
47. Alexandrov, D.V.; Ivanov, A.A.; Alexandrova, I.V. Analytical solutions of mushy layer equations describing directional solidification in the presence of nucleation. *Philos. Trans. R. Soc. A* **2018**, *376*, 20170217. [CrossRef]
48. Toropova, L.V.; Alexandrov, D.V. Dynamical law of the phase interface motion in the presence of crystals nucleation. *Sci. Rep.* **2022**, *12*, 10997. [CrossRef]
49. Alexandrov, D.V.; Toropova, L.V. The role of incoming flow on crystallization of undercooled liquids with a two-phase layer. *Sci. Rep.* **2022**, *12*, 17857. [CrossRef]
50. Makoveeva, E.V.; Alexandrov, D.V. Effects of external heat/mass sources and withdrawal rates of crystals from a metastable liquid on the evolution of particulate assemblages. *Eur. Phys. J. Spec. Top.* **2019**, *228*, 25–34. [CrossRef]